Emergent collective heat engines from neighborhood-dependent thermal reservoirs

Carlos E. Fiore
Universidade de São Paulo, Instituto de Física, Rua do Matão, 1371, 05508-090 São Paulo, SP, Brazil

(Received 19 September 2025; accepted 5 November 2025; published 1 December 2025)

We introduce and analyze a class of heat engines composed of interacting units, in which the thermal reservoir is associated with the neighborhood surrounding each unit. These systems can be mapped onto stochastic opinion models and are characterized by collective behavior at low temperatures, displaying different types of phase transitions, marked by spontaneous symmetry breaking and classifications that depend on topology, the neighborhood, and other ingredients. For the case of contact with two thermal baths—equivalent to each unit having $k = 4$ nearest neighbors—the system can be tuned to operate at maximum power without sacrificing the efficiency η and/or increasing dissipation $\bar{\sigma}$. All of them are related by a general expression when the worksource stems from different interaction energies. The heat engine placed in contact with more than three reservoirs is more revealing, showing that the intermediate thermal reservoir can be conveniently adjusted to achieve the desired compromise between power $\mathcal{P}$, efficiency, and dissipation. The influence of lattice topology (regular and random-regular networks), its relationship with collective operation, and distinct ratios between the temperatures of the thermal baths, has also been investigated.

DOI: 10.1103/fjtf-5glr

I. INTRODUCTION

Stochastic thermodynamics [1,2] provides a general and unified framework for addressing central issues in thermodynamics [3–5]. It not only extends the laws of thermodynamics to nonequilibrium systems operating at the nanoscale but also offers alternative interpretations, such as fluctuation theorems [6–8] and thermodynamic uncertainty relations (TURs) [9], the entropy production $\bar{\sigma}$ being a central quantity in such cases [10], distinguishing equilibrium ($\bar{\sigma} = 0$) from nonequilibrium ($\bar{\sigma} > 0$) systems. More recently, it has also been used as an indicator of nonequilibrium phase transitions [11–14].

We now turn to the thermodynamics of heat engines. This topic has aroused considerable interest, both because it extends the fundamental idea of energy conversion to the nanoscopic scale and because, in contrast to equilibrium thermodynamics, fluctuations in quantities and currents can become important [15], revealing the choice of approach or protocol as crucial for ensuring the desired performance. Generally, heat engines can be grouped into different categories, such as those operating under fixed conditions [16–18], periodically driven systems [19,20], or even a sequential/cyclic description, in which the system is placed in contact with a single thermal reservoir (isothermal process), and an instantaneous switching (adiabatic process) allows the change of thermal reservoir [21–24].

We introduce an alternative design of heat engines, based on the idea of collective behavior among units in which a well-defined thermal reservoir is associated with each local neighborhood surrounding the units. Such a description can be mapped onto opinion systems [25,26], for which a consistent thermodynamic framework was recently proposed and satisfying fluctuation theorems [27]. Opinion models are crucial in various nonequilibrium systems, such as complex social processes, population dynamics, decision making, elections, the spreading of fake news/rumors, and others [28]. Their simplest forms are those composed of two states per agent—the voter [29] and majority vote (MV) models [30]—which constitute remarkable examples and exhibit universal features of nonequilibrium phase transitions. The simplest case (the MV model) involves an interaction mechanism in which an agent tends to align (follow) its opinion based on the majority opinion of its nearest neighbors [30–32]. Subsequent generalizations of the MV model have attracted significant interest, taking into account the influence of network topology [31,32], the inclusion of distinct types of noise [33,34], more states per agent [35,36], inertial effects [36–38], and other cooperative effects [39]. As a consequence, the classification of phase transitions and the universality class can change.

We perform a careful analysis, taking into account the influence of distinct elements such as the worksource, neighborhood, interaction topology, and the relationship between temperatures. Our results show that the present approach is capable of designing heat engines that operate at maximum power with desired efficiency and controlled dissipation.

This paper is organized as follows: Model thermodynamics, the neighborhood thermal reservoirs, and its relationship with opinion models are presented in Sec. II. The main results for two and three thermal baths are shown in Sec. III and conclusions are addressed in Sec. IV.

II. MODEL AND THERMODYNAMICS

The systems we are dealing with are defined on a lattice of size N, and each microscopic configuration σ corresponds to a collection of N spins, $\sigma \equiv (\sigma_1, \sigma_2, \ldots, \sigma_i, \ldots, \sigma_N)$, with σ_i denoting the spin variable at site i, which takes the values ± 1 depending on whether the spin is "up" ($\sigma_i = 1$) or "down" ($\sigma_i = -1$). Its dynamics is governed by the following master

equation:

$$\frac{d}{dt}P(\sigma,t)=\sum_{i=1}^{N}\{w_i(\sigma^i)P(\sigma^i,t)-w_i(\sigma)P(\sigma,t)\}, \quad (1)$$

where $w_i(\sigma)$ comprises the transition rate at which each site i changes its spin from σ_i to $-\sigma_i$. For a lattice in which each unit (spin) has k neighbors, the thermodynamic description is set up by assuming that each transition rate $w_i(\sigma)$ can be decomposed into $k/2$ distinct (and mutually exclusive) components, each associated with a given thermal reservoir. From Eq. (1), $w_i(\sigma)$ is then written as

$$w_i(\sigma)=\sum_{\ell}w_{\ell i}(\sigma) \quad (\ell=2,4,\ldots,k), \quad (2)$$

where each term $w_{\ell i}(\sigma)$ assumes the Glauber form [2]

$$w_{\ell i}(\sigma)=\frac{\alpha_\ell}{2}\left\{1-\tanh\left[\frac{\beta_\ell}{2}(\Delta E_\ell-\theta_\ell F_\ell)\right]\right\}, \quad (3)$$

where α_ℓ is a constant, $\Delta E_\ell=E_\ell(\sigma^i)-E_\ell(\sigma)$ denotes the energy difference between configurations σ and σ^i, which are placed in contact with the ℓth thermal reservoir, with reciprocal temperature β_ℓ, and $\theta_\ell F_\ell$ accounts for the contribution of a worksource with strength F_ℓ and $\theta_\ell=\pm1$ depending on the local transition. Our reservoir approach implies that all neighborhoods with the same $|\ell|$ have the same temperature β_ℓ. For systems with "up-down" Z_2 symmetry, the energy can be generically expressed according to the Ising-like form [40]

$$E_\ell(\sigma)=-J_\ell\sum_{(i,j)}\sigma_i\sigma_j-H_\ell\sum_{i=1}^{N}\sigma_i, \quad (4)$$

where J_ℓ represents the interaction energy over a neighborhood of k spins and H_ℓ is the magnetic field. The system presents two ferromagnetic phases at low temperatures, and a ferromagnetic-paramagnetic phase transition takes place as the temperature is raised.

We now proceed with the thermodynamic description. Starting with the entropy definition $S=-\langle\ln P(\sigma)\rangle$ (we adopt the convention $k_B=1$), its time derivative dS/dt leads to the following expression for the entropy production in the nonequilibrium steady state (NESS), $P(\sigma,t)\to p^{\rm st}(\sigma)$ [11]:

$$\bar{\sigma}=\sum_i\left\langle w_i(\sigma)\ln\left(\frac{w_i(\sigma)}{w_i(\sigma^i)}\right)\right\rangle. \quad (5)$$

The first law of thermodynamics is established by taking the time derivative of the mean energy $U=\langle E(\sigma)\rangle$, given by $dU/dt=\sum_\ell\Phi_\ell+\mathcal{P}$, where Φ_ℓ denotes the heat exchanged with the ℓth thermal reservoir, defined as

$$\Phi_\ell=\sum_i\langle[E_\ell(\sigma^i)-E_\ell(\sigma)-\theta_\ell F_\ell]w_{\ell i}(\sigma)\rangle. \quad (6)$$

The expression for the power $\mathcal{P}$ can be obtained from the first law of thermodynamics in the NESS ($dU/dt=0$) as $\mathcal{P}=-\sum_\ell\Phi_\ell$. In particular, $\mathcal{P}=0$ when the J_ℓ's are equal and $F_\ell=0$ for all ℓ.

From Eq. (3), one obtains the ratio $w_{\ell i}(\sigma)/w_{\ell i}(\sigma^i)$ for each thermal reservoir ℓ, consistent with the local detailed balance:

$$\frac{w_{\ell i}(\sigma)}{w_{\ell i}(\sigma^i)}=e^{-\beta_\ell[E_\ell(\sigma^i)-E_\ell(\sigma)-\theta_\ell F_\ell]}. \quad (7)$$

By inserting Eq. (7) into Eq. (5) and taking into account that thermal reservoirs are mutually exclusive, the entropy production can be expressed as $\bar{\sigma}=\sum_\ell\bar{\sigma}_\ell$, where each entropy flux component $\bar{\sigma}_\ell$ is given by

$$\bar{\sigma}_\ell=\sum_\sigma p^{\rm st}(\sigma)\sum_i w_{\ell i}(\sigma)\ln\frac{w_{\ell i}(\sigma)}{w_{\ell i}(\sigma^i)}. \quad (8)$$

It is straightforward to see that the entropy flux component $\bar{\sigma}_\ell$ is related to the exchanged heat Φ_ℓ by a Clausius-like relation, $\bar{\sigma}_\ell=-\beta_\ell\Phi_\ell$, where Φ_ℓ is given by Eq. (6).

Generic and majority vote models. We now turn to the relationship between this class of heat engines and opinion models. Although the thermodynamics of opinion systems is rather unconventional, their key features and phase transitions, above all the behavior of the entropy production have been set up recently [11,30,34,41]. Moreover, it offers a simple way to link the different temperatures governing the dynamics by means of a common parameter (alignment probability rate).

The generic vote model has a transition rate expressed the form $w_i(\sigma)=[1-\sigma_i g(\ell)]/2$, where $g(\ell)$ depends on the neighborhood ℓ and is an odd function, constrained between 0 and 1. Its simplest case is the majority vote (MV) model [30], in which $g(\ell)=\mathrm{sgn}(\ell)$ for all ℓ. Transition rates for the MV are then given by

$$w_i(\sigma)=\tfrac{1}{2}\{1-(1-2f)\sigma_i\mathrm{sgn}(\ell)\}, \quad (9)$$

meaning the spin σ_i tends to align itself with the local majority of its neighborhood with probability $1-f$, and with complementary probability f, the majority rule is not followed. Equation (9) is valid for all values of f in the interval $0\leqslant f\leqslant 1/2$.

From Eq. (9), the ratio between $w_i(\sigma)$ and its reverse $w_i(\sigma^i)$ is given by

$$\ln\frac{w_i(\sigma)}{w_i(\sigma^i)}=-\sigma_i\,\mathrm{sgn}(\ell)\ln\left(\frac{1-f}{f}\right). \quad (10)$$

To relate β_ℓ's and f, we take the energy difference due to the spin flip, given by $\Delta E_\ell=2\sigma_i|\ell|\mathrm{sgn}(\ell)$ for the Ising model by setting $H_\ell=0$, such latter assumption because $\mathrm{sgn}(\ell)=-\mathrm{sgn}(-\ell)$ for any ℓ. By choosing for simplicity $\theta_\ell=\sigma_i\mathrm{sgn}(\ell)$ and taking the logarithm of Eq. (7), it follows that

$$\ln\frac{w_{\ell i}(\sigma)}{w_{\ell i}(\sigma^i)}=-\beta_\ell\sigma_i\mathrm{sgn}(\ell)(2J_\ell|\ell|+F_\ell). \quad (11)$$

Since the transition rates associated with each thermal reservoir are mutually exclusive, a direct comparison with Eq. (10) for a given ℓ provides the evaluation of each β_ℓ given by

$$\beta_\ell=\frac{1}{(2J_\ell|\ell|+F_\ell)}\ln\left(\frac{1-f}{f}\right), \quad (12)$$

where it follows that $\beta_2J_2=2\beta_4J_4=3\beta_6J_6\ldots=k\beta_kJ_k/2$ for $F_\ell=0$ and $\beta_2(4J_2+F_2)=\beta_4(8J_4+F_4)=\beta_6(12J_6+F_6)\ldots$ for $F_\ell\neq0$. Note that the right-hand side of Eq. (12) establishes a relationship among all the temperatures involved and will be taken into account in the subsequent analysis.

To extend the present description to a generic voter model, it is required the knowledge of $g(\ell)$ for each ℓ. By taking for simplicity $k=4$ and $F_\ell=0$, $g(\ell)$ can be expressed as $g(0)=0$, $|g(2)|=q$ and $|g(4)|=p$. The connection between

$\beta_2 J_2(\beta_4 J_4)$ with $q(p)$ can be obtained as before. In particular, the condition $\beta_2 J_2 = n\beta_4 J_4$ between temperatures (for $n > 2$) implies that p and q are related via expression

$$p = \frac{\left(\frac{1+q}{1-q}\right)^{2/n} - 1}{\left(\frac{1+q}{1-q}\right)^{2/n} + 1}. \tag{13}$$

In all cases, from Eq. (6) one has $\Phi_\ell = \sum_i (2J_\ell|\ell| + F_\ell)\langle\sigma_i \mathrm{sgn}(\ell) w_{\ell i}(\sigma)\rangle$, and hence the expression for $\mathcal{P}$ becomes

$$\mathcal{P} = -\sum_\ell \sum_i (2J_\ell|\ell| + F_\ell)\langle\sigma_i \mathrm{sgn}(\ell) w_{\ell i}(\sigma)\rangle. \tag{14}$$

A heat engine, providing partial conversion of energy from the hot thermal reservoir(s) $\langle\dot{Q}_2\rangle = \sum_\ell \Phi_\ell H[\Phi_\ell] > 0$ ($H[x]$ being the Heavside function) into power $\mathcal{P} < 0$ has associate efficiency η given by $\eta = -\mathcal{P}/\langle\dot{Q}_2\rangle$.

III. MAIN RESULTS

Two thermal reservoirs. The simplest heat engine corresponds to the $k = 4$ case, meaning that each unit has four nearest neighbors and is placed in contact with two different thermal reservoirs. By rewriting the heat flux in Eq. (6) as $\Phi_\ell = J_\ell \phi_\ell + F_\ell \xi_\ell$, where $\phi_\ell = 2\sum_i \langle|\ell|\mathrm{sgn}(\ell)\sigma_i w_{\ell i}(\sigma)\rangle$ and $\xi_\ell = \sum_i \langle \mathrm{sgn}(\ell)\sigma_i w_{\ell i}(\sigma)\rangle$, and taking into account that $\mathcal{P} = 0$ when $J_2 = J_4$ and $F_\ell = 0$, the first law of thermodynamics states that $\phi_2 = -\phi_4$, where $\phi_4 > 0$. The power is then written as $\mathcal{P} = (J_2 - J_4)\phi_4 - F_2\xi_2 - F_4\xi_4$. In order to investigate two different kinds of worksources, we split the analysis into two complementary cases: $J_2 \neq J_4$ and $F_2 = F_4 = 0$, and $J_2 = J_4 = J$ for $F_\ell \neq 0$. We pause to make a few comments about the former case. First, the efficiency η acquires the simple form $\eta = 1 - J_2/J_4$, which is lower than ideal efficiency $\eta_c = 1 - \beta_4/\beta_2$, also expressed as $\eta_c = 1 - J_2/(nJ_4)$ (because $\beta_2 J_2 = n\beta_4 J_4$). They are related via the relation $\eta = 1 - n + n\eta_c$, consistent with $\eta < \eta_c$ for all values of J_2 and J_4. Second, in contrast with $\mathcal{P}$ and $\langle Q_\nu\rangle$'s, $\bar{\sigma}$ is independent of J_2 and J_4 and is given by $\bar{\sigma} = -\beta_2\Phi_2 - \beta_4\Phi_4 = (\beta_2 - \beta_4)\phi_4$. Thermodynamic quantities are not independent of each other, but rather related through the identity $-\beta_2\mathcal{P}\eta_c = J_4\eta\bar{\sigma}$. Due to the fact that $\bar{\sigma}$ does not depend on the J_ℓ's, they can be adjusted to improve the power and efficiency (although $\eta < \eta_c$) without sacrificing dissipation. Third and last, since $\phi_4 > 0$, the system operates as a heat engine when $J_2 < J_4$. The roots of the power occur at $J_2 = J_4$ and $\phi_4 = 0$, the latter coinciding with the minimum of $\bar{\sigma}$, in conformity with Ref. [15]. The case of $F_\ell \neq 0$ (exemplified here for $F_2 = F_4 = F \neq 0$ and $J_2 = J_4$) is less direct. From Eq. (14), one has $\mathcal{P} = -F_2(\xi_2 + \xi_4)$ with efficiency $\eta = F(\xi_2 + \xi_4)/\Phi_4$, also bounded by the Carnot efficiency $\eta_c = 2/(4 + F)$.

Figure 1 summarizes the above results for the $\beta_2(4J_2 + F_2) = \beta_4(8J_4 + F_4)$ case (MV model) for square and random-regular (RR) topologies, both with $k = 4$ for $F_2 = F_4 = 0$ [panels (a)–(c)] and different $F_2 = F_4 \neq 0$ [panel (d)]. For convenience, all analyses are depicted in terms of the parameter f [temperatures are promptly evaluated from f via Eq. (12)]. In all cases, systems present continuous phase transitions as f is raised. They are characterized via the standard finite-size scaling analysis, through the crossing between

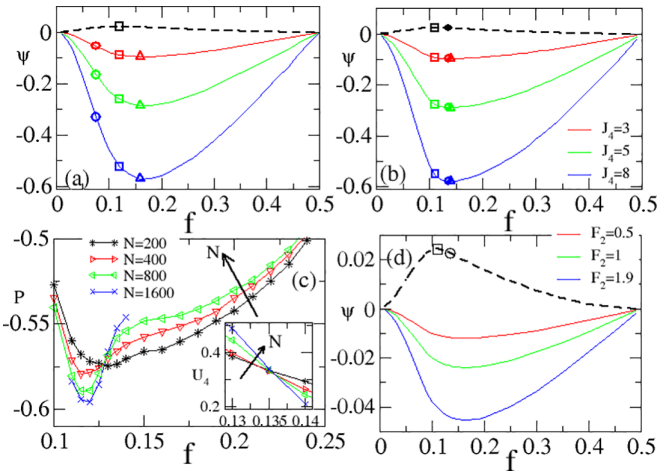

FIG. 1. Main results for the two thermal baths ($k = 4$). Panels (a) and (b) depict for $N = 100$ the power $\Psi = \mathcal{P}$ (continuous lines) and the entropy production $\Psi = \bar{\sigma}$ (dashed lines) for the MV for square ($N = L^2$) and RR topologies, respectively, for $\beta_2 J_2 = 2\beta_4 J_4$ and different sets of J_4's ($J_2 = 2$). Circles, squares, and triangles denote f_c, $f_{M\bar{\sigma}}$, and f_{mP}, respectively. Bottom left panel shows the finite size scaling of power $\mathcal{P}$ for RR topologies. Arrow indicates the increase of N. Inset: The location of critical point f_c for *RR* via crossing between curves of U_4 for different system sizes N. The right (bottom) panel shows some results ($\Psi = \mathcal{P}$ and $\bar{\sigma}$) for $J_2 = J_4$ and distinct driving strengths F_2's. In all cases, the efficiency η is constant and given by $\eta = 1 - J_2/J_4$ (a)–(c) and $\eta = F(\xi_2 + \xi_4)/\Phi_4$ (d).

curves of the reduced cumulant $U_4 = 1 - \langle m^4\rangle/(3\langle m^2\rangle^2)$ [42], where $\langle m^{\bar{n}}\rangle$ denotes the $\bar{n}$th order parameter moment, $\langle m^{\bar{n}}\rangle = \langle(\sum_{i=1}^N \sigma_i/N)^{\bar{n}}\rangle$ ($N = L^2$ and L^3 for square and cubic lattices, respectively). In particular, $\langle|m|\rangle$ and the entropy production derivative $\bar{\sigma}^* = d\bar{\sigma}/df$ scale with $\langle|m|\rangle \sim L^{-\beta/\nu}$ and $\bar{\sigma}^* \sim L^{\alpha/\nu}$ at the criticality $f = f_c$, respectively. Although $\beta/\nu = 1/8$ and $\beta/\nu = 1/2$ for square lattices and RR topologies, respectively [34,38], $\alpha/\nu = 0$ in both cases, consistent with a logarithmic divergence [11]. The value f_{mP} at which $-\mathcal{P}$ is maximum is directly related to the maximum of ϕ_4 and is different from $f_{M\bar{\sigma}}$ at which $\bar{\sigma}$ is maximum. All such points lie in the interval $f_c < f_{M\bar{\sigma}} < f_{mP}$ for square-lattice ($f_c = 0.075(1)$ [30]) topologies and change mildly as the system size is increased (not shown). On the other hand, the behavior for RR topologies is more sensitive to the system size [see, e.g., Figs. 1(a)–1(c)] and $f_{M\bar{\sigma}} < f_{mP} < f_c$ (insets) as N increases. Similar results are exemplified for different sets of $F_2 = F_4 \neq 0$ [Fig. 1(d)].

Three thermal reservoirs. The $k = 6$ case is more revealing because the system is now placed in contact with three different thermal reservoirs. As exemplified in Refs. [25,26], the thermodynamic analysis of the MV shows that $\phi_2 < 0$ and $\phi_6 > 0$ for all values of f, whereas the intermediate heat flux (ϕ_4 in such case) changes its sign at a intermediate f_0 (inset). By curbing ourselves in the case $F_\ell = 0$, together the fact that $\phi_4 = -(\phi_2 + \phi_6)$, the expressions for thermodynamic quantities can be written down in the following forms, given by $\mathcal{P} = (J_4 - J_2)\phi_2 + (J_4 - J_6)\phi_6$, $\langle Q_2\rangle = J_4\phi_4 H[\phi_4] + J_6\phi_6$ (likewise $\langle Q_1\rangle = J_4\phi_4 H[-\phi_4] + J_2\phi_2$),

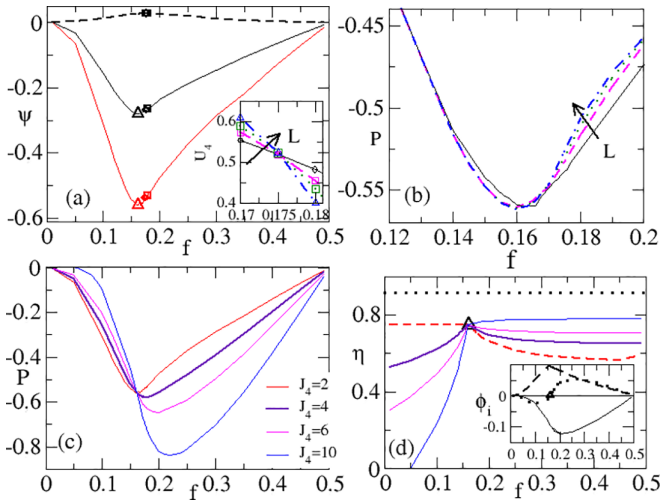

FIG. 2. The depiction of power and efficiency for the three reservoirs case ($k = 6$) for a cubic topology $\beta_2 J_2 = 2\beta_4 J_4 = 3\beta_6 J_6$. Panel (a) shows, for $L = 16$ ($N = 16^3$ sites), the behavior of $\mathcal{P}$ (continuous lines) and $\bar{\sigma}$ (dashed) for distinct f's for $J_2 = J_4 = 2$ and $J_6 = 5(8)$ for middle (bottom) curves. Triangles, squares, and circles denote $\mathcal{P}_{mP}, \mathcal{P}_{M\bar{\sigma}}$, and $\mathcal{P}_c$, respectively. Top inset: The location of f_c via crossing between U_4 curves for different system sizes. Arrow indicates the increase of L. In (b) and (c), the influence of distinct system sizes L's and intermediate J_4's ($J_2 = 2$ and $J_6 = 8$), respectively, for distinct f's. The corresponding efficiency curves of panel (c) are reported in (d). Dotted and dashed lines correspond to the ideal efficiency η_c and for $J_2 = J_4$, respectively. Bottom inset: The fluxes ϕ_ℓ's versus f. Triangle denotes the value f_0 in which ϕ_4 vanishes.

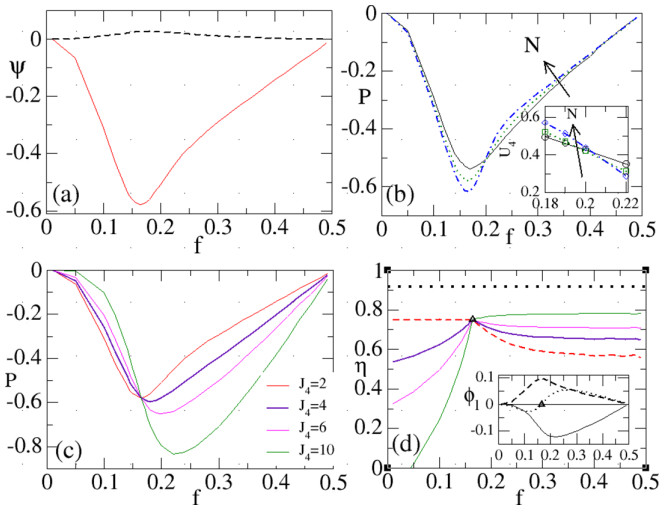

FIG. 3. The same as Fig. 2 but for RR topologies as $k = 6$.

$\bar{\sigma} = (\beta_4 - \beta_2)\phi_2 + (\beta_4 - \beta_6)\phi_6$. The efficiency η then reads

$$\eta = \frac{(J_2 - J_4)\phi_2 + (J_6 - J_4)\phi_6}{J_4\phi_4 H[\phi_4] + J_6\phi_6}, \tag{15}$$

lower than $\eta \leqslant \eta_c = 1 - J_2/(3J_6)$ (for the MV), for all values of J_ℓ's (as should be). We see that $\mathcal{P}$ presents three different roots, at $J_2 = J_4 = J_6$ (absence of a heat-engine behavior), $\phi_2 = \phi_6 = 0$ (corresponding to the minimum of dissipation for the MV $f = 0$ or $f = 1/2$), and $(J_4 - J_2)/(J_4 - J_6) = -\phi_6/\phi_2$. We also exemplify the three thermal baths case for $\beta_2 J_2 = 2\beta_4 J_4 = 3\beta_6 J_6$ (MV case), as summarized in Figs. 2 and 3. As the two thermal baths previous case, the system also yields a continuous phase transition, presenting different critical exponents for regular (cubic) lattices $\beta = 0.32630(22)$, $\nu = 0.629912(86)$ ($d = 3$) [43], and $\beta/\nu = 1/2$ for RR (like $k = 4$) [34]. Unlike the two thermal baths case, in which $\mathcal{P}$ curves solely differ by a factor $J_4 - J_2$ with fixed η, the presence of an intermediate thermal reservoir can be conveniently chosen for improving the power and efficiency for both lattice topologies. Also, maximum powers $-\mathcal{P}_{mP}'$s also deviate for larger values f (the system can be constrained in the disordered phase as $N \to \infty$) as J_4 increases. The behavior of η is also different as a consequence of ϕ_4 changing its sign at f_0 ($f_0 \approx 0.162$ for both cubic and RR, respectively). For $f < f_0$, η solely depends on ϕ_2 and ϕ_6 and it is given by

$$\eta = 1 - \frac{J_4}{J_6} + \frac{J_2 - J_4}{J_6}\frac{\phi_2}{\phi_6}. \tag{16}$$

Note that $\eta = 1 - J_4/J_6$ for $J_2 = J_4$, as depicted in Figs. 2(d) and 3(d) (dashed lines). By choosing suited values of J_4, the existence of an intermediate thermal reservoir not only can improve the power, but also the efficiency, as depicted in Figs. 2(d) and 3(d).

Pair mean-field description for the power and dissipation. In order to provide additional insights about such class of heat engines, we investigate the system behavior via the mean-field approach for $k = 4$ by taking the correlation of two sites, also known as pair mean-field approximation [2,25]. At this level of approximation, all quantities can be expressed in terms of $m = \langle\sigma_i\rangle$ and the two-site correlation, and $r = \langle\sigma_0\sigma_i\rangle$. To see this, let $P(\sigma_1, \sigma_2, \sigma_3, \sigma_4|\sigma_0)$ be the conditional probability with σ_0 and σ_i being the spin of the central site and its $k = 4$ nearest neighbors, respectively. It can be written as $P(\sigma_1, \sigma_2, \sigma_3, \sigma_4|\sigma_0) = \prod_i P(\sigma_i|\sigma_0)$, where $P(\sigma_i|\sigma_0) = P(\sigma_i, \sigma_0)/P(\sigma_0)$. They are related with m and r through relations as $P(\sigma_0) = (1 + m\sigma_0)/2$ and $P(\sigma_i, \sigma_0) = [1 + m(\sigma_0 + \sigma_i) + r\sigma_0\sigma_i]/4$, respectively. In order to find the steady solutions for thermodynamic quantities, we take the time evolution of m and r, expressed in terms of correlations of type $\langle\sigma_0\sigma_1 \ldots \sigma_n\rangle$ and $\langle\sigma_1 \ldots \sigma_n\rangle$. From Ref. [25], we see they can be conveniently written in the following forms: $\langle\sigma_0\sigma_1 \ldots \sigma_n\rangle = (A_n - B_n)/2$ and $\langle\sigma_1 \ldots \sigma_n\rangle = (A_n + B_n)/2$, respectively, where

$$A_n = \frac{(m + r)^n}{(1 + m)^{n-1}} \quad \text{and} \quad B_n = \frac{(m - r)^n}{(1 - m)^{n-1}}. \tag{17}$$

We arrive at the following equations for m and r:

$$\frac{dm}{dt} = -m - 4am + 2b(A_3 + B_3) \tag{18}$$

and

$$\frac{dr}{dt} = -2r + 2a + 3(a + b)(A_2 + B_2) + b(A_4 + B_4), \tag{19}$$

respectively. Parameters a and b are simpler for $\beta_2 J_2 = 2\beta_4 J_4$ (MV for $F_\ell = 0$) and given by $b = -3a$, where $b = -(1 - 2f)/8$. For the generic case $\beta_2 J_2 = n\beta_4 J_4$, one has $a = (p + 2q)/8$ and $b = (p - 2q)/8$, where p and q were described

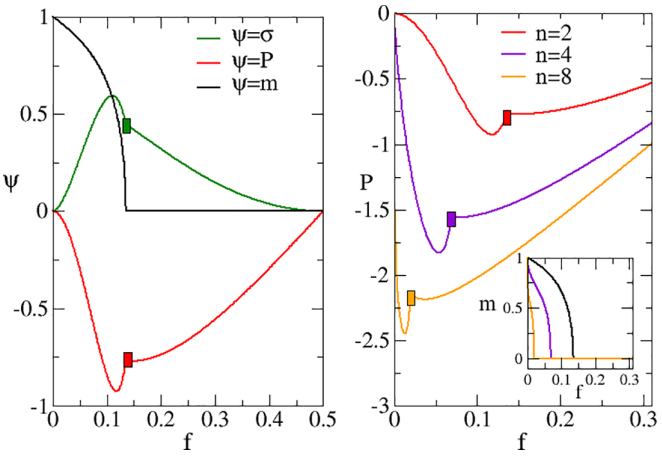

FIG. 4. Left: For $\beta_2 J_2 = 2\beta_4 J_4$ (MV) and $F'_\ell s = 0$, the depiction of $\Psi = m, \mathcal{P}$ and $\Psi = \bar{\sigma}$ for the pair approximation for $k = 4$. Right: The comparison between $\mathcal{P}'$s for different n's. Quantities have been expressed in terms of $f = (1-q)/2$. The behavior of thermodynamic quantities is marked by a kink (symbol ■) at the phase transition, the disordered phase being at the right. Inset: The corresponding behavior for m's. Parameters: $J_2 = 2$ and $J_4 = 8$.

previously. As stated previously, quantities can be solely expressed in terms of ϕ_4 for $k = 4$, $\mathcal{P} = (J_2 - J_4)\phi_4$, and $\bar{\sigma} = (\beta_2 - \beta_4)\phi_4$, where flux ϕ_4 reads

$$\phi_4 = A_3 - B_3 - a(A_4 + B_4) - 3(a+b)(A_2 + B_2) - 2b. \tag{20}$$

The steady state solution characterizing the ordered phase is found by solving numerically Eqs. (18) and (19). On the other hand, they become simpler in the disordered phase, in which $m = 0$ and $r = a + 3(a+b)r^2 + br^4$, and the flux ϕ_4 is given by $\phi_4 = 2r^3 - 6r^2(a+b) - 2ar^4 - 2b$ or equivalently $\phi_4 = [8r^3 - p(r^4 + 6r^2 + 1) - 2q(r^4 - 1)]/4$.

Figure 4 summarizes above discoveries for $m, \mathcal{P}$, and $\bar{\sigma}$ for $n = 2$ as well as a comparison of $\mathcal{P}$ for distinct $n's$. As can be seen, it reproduces previous similar trademarks of a heat engine in both ordered and disordered phases, in which maximum power and dissipation yields at the ordered phase, consistent with the collective behavior improving the system performance. Although the values of $f_{M\bar{\sigma}}$, f_{mP}, and f_c obtained from mean-field theory (MFT) are different from the estimates on square lattices [Fig. 1(a)], they follow the same ordering ($f_{M\bar{\sigma}} < f_{mP} < f_c$) and are very close to those for the RR case [Figs. 1(b) and 1(c)]. In contrast to previous topologies, both $\mathcal{P}$ and $\bar{\sigma}$ exhibit a kink at the phase transition. Also, both $\mathcal{P}$ and its maximum values $-\mathcal{P}_{mP}$ increase as n (larger difference of temperatures) goes up. However, the ordered phase is substantially shortened in this case.

IV. CONCLUSIONS

We presented an alternative kind of nonequilibrium thermal engines operating collectively, based on the idea of a well defined thermal reservoir due to the spin neighborhood. Unlike other kinds of collective heat engines [17], the system exhibits a heat engine behavior which can be optimized in both ordered and disordered phases. We derived a general relation between power, efficiency, and dissipation for the two thermal reservoirs case. Also in contrast with other examples of collective systems [18], results are similar for different topologies, suggesting that it does not play a fundamental role upon the system performance. Remarkably, the optimized points (maximum power and dissipation) and the critical point obtained for RR topologies lie very close to those obtained from the pair MFT. The three thermal baths exhibit richer features in which the intermediate thermal reservoirs can be properly adjusted ensuring the improving of power and efficiency. The connection with different kinds of voter models was also considered and exemplified, highlighting different routes for improving the power and efficiency.

ACKNOWLEDGMENTS

We acknowledge Gustavo Forão for the reading of the manuscript and insightful suggestions. The financial support from Brazilian agencies CNPq and FAPESP under Grants No. 300244/2025-8, No. 309311/2021-7, No. 2023/17704-2, No. 2024/08157-0, No. 2024/03763-0, and No. 2022/15453-0, respectively, is also acknowledged.

DATA AVAILABILITY

The data are not publicly available. The data are available from the authors upon reasonable request.

[1] U. Seifert, Rep. Prog. Phys. **75**, 126001 (2012).
[2] T. Tomé and M. J. De Oliveira, *Stochastic Dynamics and Irreversibility* (Springer, 2015).
[3] I. Prigogine, *Introduction to Thermodynamics of Irreversible Processes* (Interscience, New York, 1965).
[4] S. R. de Groot and P. Mazur, *Non-Equilibrium Thermodynamics* (North-Holland, Amsterdam, 1962).
[5] C. Van den Broeck and M. Esposito, Phys. A **418**, 6 (2015).
[6] C. Jarzynski, Phys. Rev. Lett. **78**, 2690 (1997).
[7] O.-P. Saira, Y. Yoon, T. Tanttu, M. Möttönen, D. Averin, and J. P. Pekola, Phys. Rev. Lett. **109**, 180601 (2012).
[8] K. Proesmans and C. Van den Broeck, Europhys. Lett. **119**, 20001 (2017).
[9] A. C. Barato and U. Seifert, Phys. Rev. Lett. **114**, 158101 (2015).
[10] J. Schnakenberg, Rev. Mod. Phys. **48**, 571 (1976).
[11] C. F. Noa, P. E. Harunari, M. de Oliveira, and C. Fiore, Phys. Rev. E **100**, 012104 (2019).
[12] T. Martynec, S. H. Klapp, and S. A. Loos, New J. Phys. **22**, 093069 (2020).
[13] C. E. Fiore, P. E. Harunari, C. F. Noa, and G. T. Landi, Phys. Rev. E **104**, 064123 (2021).
[14] B. Nguyen and U. Seifert, Phys. Rev. E **102**, 022101 (2020).
[15] G. A. L. Forão, J. Berx, and C. E. Fiore, New J. Phys. **27**, 074605 (2025).

[16] H. Vroylandt, M. Esposito, and G. Verley, Europhys. Lett. **120**, 30009 (2017).
[17] F. S. Filho, G. A. L. Forão, D. M. Busiello, B. Cleuren, and C. E. Fiore, Phys. Rev. Res. **5**, 043067 (2023).
[18] I. N. Mamede, K. Proesmans, and C. E. Fiore, Phys. Rev. Res. **5**, 043278 (2023).
[19] K. Proesmans, Y. Dreher, M. Gavrilov, J. Bechhoefer, and C. Van den Broeck, Phys. Rev. X **6**, 041010 (2016).
[20] I. N. Mamede, P. E. Harunari, B. A. N. Akasaki, K. Proesmans, and C. E. Fiore, Phys. Rev. E **105**, 024106 (2022).
[21] A. L. L. Stable, C. E. F. Noa, W. G. C. Oropesa, and C. E. Fiore, Phys. Rev. Res. **2**, 043016 (2020).
[22] C. E. F. Noa, A. L. L. Stable, W. G. C. Oropesa, A. Rosas, and C. E. Fiore, Phys. Rev. Res. **3**, 043152 (2021).
[23] P. E. Harunari, F. S. Filho, C. E. Fiore, and A. Rosas, Phys. Rev. Res. **3**, 023194 (2021).
[24] A. Rosas, C. Van den Broeck, and K. Lindenberg, Phys. Rev. E **96**, 052135 (2017); **97**, 062103 (2018); G. A. L. Forão, F. S. Filho, B. A. N. Akasaki, and C. E. Fiore, *ibid.* **110**, 054125 (2024).
[25] T. Tomé, C. E. Fiore, and M. J. de Oliveira, Phys. Rev. E **107**, 064135 (2023).
[26] F. Hawthorne, P. E. Harunari, M. J. de Oliveira, and C. E. Fiore, Entropy **25**, 1230 (2023).
[27] G. E. Crooks, Phys. Rev. E **60**, 2721 (1999).
[28] C. Castellano, S. Fortunato, and V. Loreto, Rev. Mod. Phys. **81**, 591 (2009).
[29] T. M. Liggett, *Interacting Particle Systems* (Springer, New York, 1995).
[30] M. J. de Oliveira, J. Stat. Phys. **66**, 273 (1992).
[31] L. F. Pereira and F. B. Moreira, Phys. Rev. E **71**, 016123 (2005).
[32] H. Chen, C. Shen, G. He, H. Zhang, and Z. Hou, Phys. Rev. E **91**, 022816 (2015).
[33] A. R. Vieira and N. Crokidakis, Phys. A **450**, 30 (2016).
[34] J. Encinas, H. Chen, M. M. de Oliveira, and C. E. Fiore, Phys. A **516**, 563 (2019).
[35] A. Brunstein and T. Tomé, Phys. Rev. E **60**, 3666 (1999).
[36] H. Chen, C. Shen, H. Zhang, G. Li, Z. Hou, and J. Kurths, Phys. Rev. E **95**, 042304 (2017).
[37] P. E. Harunari, M. de Oliveira, and C. E. Fiore, Phys. Rev. E **96**, 042305 (2017).
[38] J. M. Encinas, P. E. Harunari, M. de Oliveira, and C. E. Fiore, Sci. Rep. **8**, 9338 (2018).
[39] I. V. Oliveira, C. Wang, G. Dong, R. Du, C. E. Fiore, A. L. Vilela, and H. E. Stanley, Chaos, Soliton Fract. **181**, 114694 (2024).
[40] J. M. Yeomans, *Statistical Mechanics of Phase Transitions* (Clarendon Press, Oxford, 1992).
[41] L. Crochik and T. Tomé, Phys. Rev. E **72**, 057103 (2005).
[42] D. Landau and K. Binder, *A Guide to Monte Carlo Simulations in Statistical Physics* (Cambridge University Press, 2021).
[43] S. Kazmin and W. Janke, Phys. Rev. B **105**, 214111 (2022).